# Rational design of helical architectures

**Dwaipayan Chakrabarti, Szilard N. Fejer, and David J. Wales[1]**

University Chemical Laboratories, Lensfield Road, Cambridge CB2 1EW, United Kingdom

Edited by Angel E. Garcia, Rensselaer Polytechnic Institute, Troy, NY, and accepted by the Editorial Board September 22, 2009 (received for review June 16, 2009)

**Nature has mastered the art of creating complex structures through self-assembly of simpler building blocks. Adapting such a bottom-up view provides a potential route to the fabrication of novel materials. However, this approach suffers from the lack of a sufficiently detailed understanding of the noncovalent forces that hold the self-assembled structures together. Here we demonstrate that nature can indeed guide us, as we explore routes to helicity with achiral building blocks driven by the interplay between two competing length scales for the interactions, as in DNA. By characterizing global minima for clusters, we illustrate several realizations of helical architecture, the simplest one involving ellipsoids of revolution as building blocks. In particular, we show that axially symmetric soft discoids can self-assemble into helical columnar arrangements. Understanding the molecular origin of such spatial organisation has important implications for the rational design of materials with useful optoelectronic applications.**

anisotropic interactions | columnar arrangements | helix | self-assembly

Nature provides ubiquitous examples of helical architecture with diverse functions. Helical structures are common structural motifs in biomolecules and are involved in the storage of genetic information (1). They are also important in solid- and liquid–crystal engineering for fabricating functional materials with useful optoelectronic applications (2–5). For example, discotic molecules in crystalline or liquid crystalline states often exhibit helical order in columnar arrangements (2–6), and such materials are attractive for use in optoelectronic devices because of the exceptional 1D charge-carrier mobilities along the columns (2–4). A common route to induce helicity in columnar arrangements is inclusion of chiral centers in discotic molecules (7). Helical columnar arrangements have also been realized in a few cases with achiral discotic molecules (8, 9), although no general strategy seems to have emerged.

Self-assembly is nature's prescription for the creation of complex structures from simpler building blocks (10, 11). Although many novel building blocks have been discovered for self-assembly, differing in shape, composition, and functionality (12, 13), the basic rules that govern this process are not yet understood in sufficient detail to realize target structures routinely through a priori design of building blocks. Here we ask the specific question: Can we learn from nature how to design building blocks that self-assemble into helical structures? In seeking a guiding principle from nature for obtaining helical architectures, we considered DNA, in which two competing length scales exist, one characterizing the distance between consecutive nucleotides in the sugar-phosphate backbone and the other governing the stacking of the base pairs (1). The present contribution thus explores realizations of helical architectures with achiral building blocks driven by the interplay between two competing length scales. To this end, we characterize global minima (14–16) for clusters bound by generic intermolecular potentials. (See the *SI Appendix* for a detailed description of the potentials describing the interactions between the building blocks and Fig. S1 of the *SI Appendix*.)

**Section Results and Discussion.** We first consider assembly of asymmetric dipolar dumbbells driven by an electric field, inspired by recent experimental work that used asymmetric colloidal dumbbells linked at the waist by magnetic belts (17). We model the asymmetric dipolar dumbbells by using multiple interaction sites within a rigid-body framework (18). Each dumbbell involves two spherical lobes, modeled by Lennard–Jones (LJ) sites (labeled 1 and 2), and a point dipole directed across the axis between the lobes. The total energy of a system of $N$ dumbbells in an electric field $\mathbf{E}$ is

$$U^{DB} = \sum_{I=1}^{N-1}\sum_{J=I+1}^{N}\sum_{i\in I}^{1,2}\sum_{j\in J}^{1,2} 4\varepsilon_{ij}\left[\left(\frac{\sigma_{ij}}{r_{ij}}\right)^{12} - \left(\frac{\sigma_{ij}}{r_{ij}}\right)^{6}\right] + \sum_{I=1}^{N-1}\sum_{J=I+1}^{N}\frac{\mu_D^2}{r_{IJ}^3}[(\hat{\boldsymbol{\mu}}_I\cdot\hat{\boldsymbol{\mu}}_J) - 3(\hat{\boldsymbol{\mu}}_I\cdot\hat{\mathbf{r}}_{IJ})(\hat{\boldsymbol{\mu}}_J\cdot\hat{\mathbf{r}}_{IJ})] - \mu_D\sum_{I=1}^{N}\hat{\boldsymbol{\mu}}_I\cdot\mathbf{E}. \quad [1]$$

Here, $\mathbf{r}_I$ is the position vector for the point dipole on dumbbell $I$, $\hat{\mu}_I$ is the unit vector defining the direction of the dipole moment whose magnitude is $\mu_D$, $\mathbf{r}_{IJ} = \mathbf{r}_I - \mathbf{r}_J$ is the separation vector between dipoles on dumbbells $I$ and $J$ with magnitude $r_{IJ}$, $\hat{\mathbf{r}}_{IJ} = \mathbf{r}_{IJ}/r_{IJ}$, and $r_{ij}$ is the separation between LJ sites $i$ and $j$. The units of energy and length are chosen as the LJ parameters $\varepsilon_{11}$ and $\sigma_{11}$, respectively. For the LJ interactions, we set $\varepsilon_{11} = \varepsilon_{22} = \varepsilon_{12} = 1$ and $\sigma_{11} = 1$. $\sigma_{22} < 1$ was varied to explore the effects of asymmetry with $\sigma_{12} = (\sigma_{11} + \sigma_{22})/2$. With the lobes characterized as spheres with diameters $\sigma_{11}$ and $\sigma_{22}$, we define an asymmetry parameter $\alpha = \sigma_{11}/\sigma_{22}$. The direction of the electric field $\mathbf{E} = (0, 0, E)$ was held fixed along the $z$ axis of the space-fixed frame as its strength, $E$, was varied. $\mu_D$ is then in reduced units of $(4\pi\varepsilon_0\varepsilon_{11}\sigma_{11}^3)^{1/2}$ and $E$ is in $[\varepsilon_{11}/(4\pi\varepsilon_0\sigma_{11}^3)]^{1/2}$, where $\varepsilon_0$ is the permittivity of free space. Although a number of parameters are involved here, we restrict ourselves to varying only $\sigma_{22} < 1$, $\mu_D$, and $E$ to manipulate the two competing interactions.

In Fig. 1, we illustrate putative global minima for clusters of asymmetric dumbbells under different conditions. We first focus on the cluster size $n = 6$ with the asymmetry parameter $\alpha$ fixed to 2. A distorted octahedral packing results when dipolar interactions are absent (Fig. 1 *A* and *E*). In the presence of point dipoles, we observe a slightly distorted hexagonal arrangement of the dipoles, thus allowing approximate octahedral packing for the smaller spheres (Fig. 1 *B* and *F*). When an electric field is applied, a single helical strand grows along the direction of the field (Fig. 1 *C*, *D*, *G*, and *H*). The asymmetry of the dumbbells, which controls the steric factor, proves to be crucial for helix

Author contributions: D.C. and D.J.W. designed research; D.C. and S.N.F. performed research; D.C. and S.N.F. analyzed data; and D.C. and D.J.W. wrote the paper.

The authors declare no conflict of interest.

This article is a PNAS Direct Submission. A.E.G. is a guest editor invited by the Editorial Board.

[1]To whom correspondence should be addressed: E-mail: dw34@cam.ac.uk.

This article contains supporting information online at www.pnas.org/cgi/content/full/0906676106/DCSupplemental.

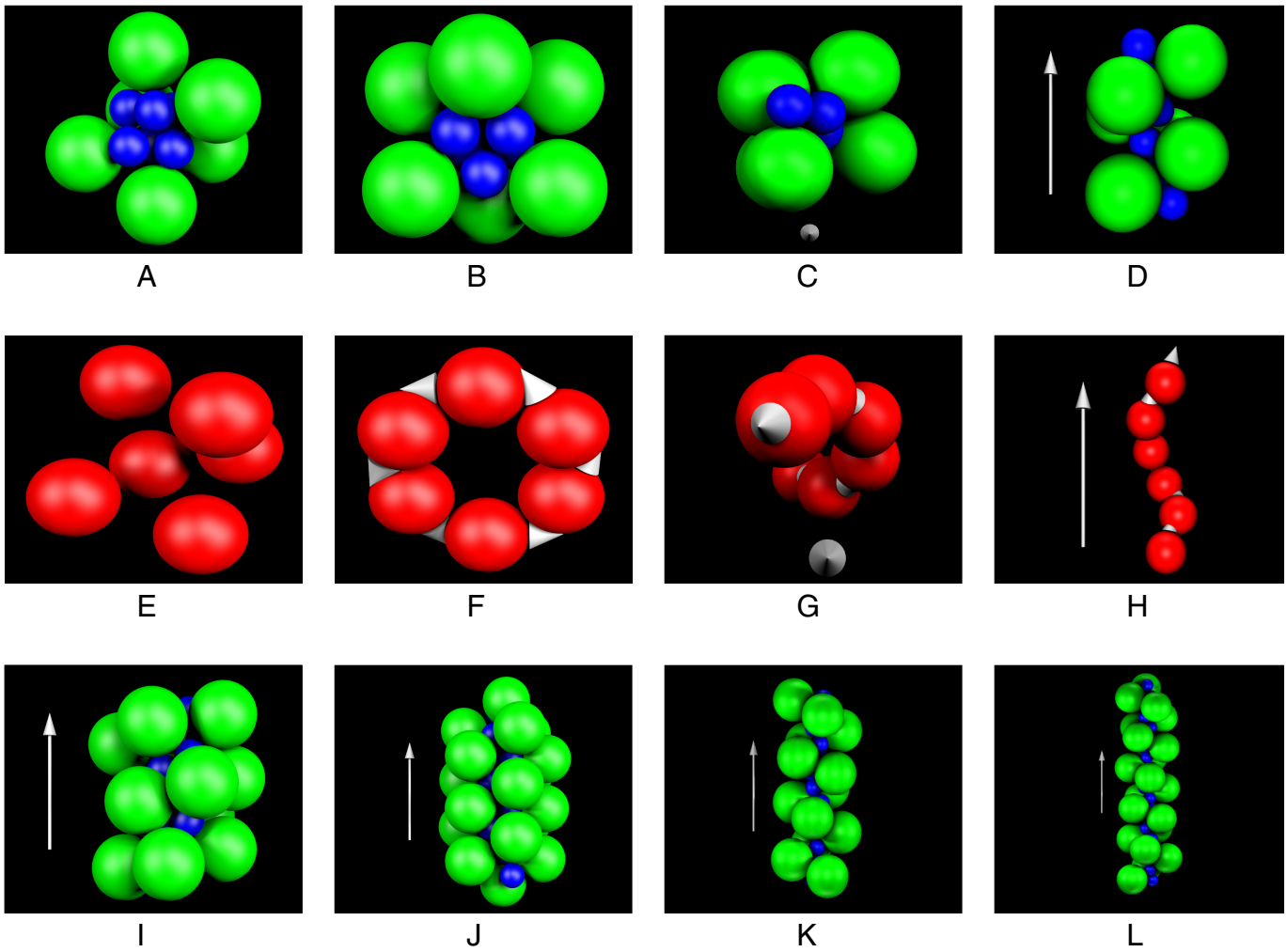


**Fig. 1.** Global minima for clusters of asymmetric dumbbells. (*A–D*) Structures obtained for $n = 6$ asymmetric dumbbells with the size ratio between the spherical lobes, characterized by the asymmetry parameter $\alpha$, set to 2. (*A*) Apolar dumbbells. (*B*) Dipolar dumbbells. (*C* and *D*) Dipolar dumbbells in the presence of an applied electric field (top view and side view, respectively). (*E–H*) The same structures as in *A–D* in the same order but, for clarity, depicting only the position of the point dipole on the dumbbell axis. (*I–L*) Structures for larger cluster sizes (side views). (*I*) $n = 13$ for $\alpha = 2$; (*J*) $n = 20$ for $\alpha = 2$; (*K*) $n = 13$ for $\alpha = 2.5$; (*L*) $n = 20$ for $\alpha = 2.5$. When dipolar interactions are present, the dipole vectors are also shown. Emergence of helicity under the applied field is clearly evident, especially in the reduced representations. Here the dipole moment $\mu_D = 0.7$ and the electric field strength $E = 5$. In *C* and *D* and *G–L*, the arrows indicate the field direction.

formation in this case, competing against the dipole interactions with the field (see *SI Text* and Fig. S2 of the *SI Appendix*). It is clear that the dumbbells tend to align perpendicular to the field because of the dipolar interactions. However, competition with a second length scale that controls the steric interactions causes a rototranslational axis to appear in the growth process. Although particles interacting via a single-site LJ plus a point-dipole (Stockmayer) potential tend to form strings (19, 20), helical order has not been reported for this system. In the presence of an applied electric field, linear chains are observed instead for clusters of Stockmayer particles as well as for symmetric dumbbells (Fig. S2 of the *SI Appendix*), when the interactions of the dipoles with the field are sufficiently strong. Hence, competition between two length scales is crucial in driving helix formation for asymmetric dipolar dumbbells in an applied field: We find helical strands only when the asymmetry parameter is between ≈2 and 2.8 and the field is strong enough ($E > 2$ for $\mu_D = 0.7$). When $\alpha = 2$, a second strand emerges for $n = 13$, as shown in Fig. 1*I*, and the two strands do not run in parallel. For $n = 20$, although the three strands we observe are nearly parallel (Fig. 1*J*), the radius of the helical strand is much diminished. On the contrary, a single helical strand is observed for $n = 13$ as well as $n = 20$ when $\alpha = 2.5$ (Fig. 1 *K* and *L*); see also Fig. S3 of the *SI Appendix*. When the restricted parameter space is explored, the well-defined single helical strand for $n = 20$ is found to be robust over a wide parameter range (see *SI Appendix*). It is thus apparent that one can tune the two length scales for these anisotropic interactions to design helical architectures.

An ellipsoid of revolution is perhaps the simplest building block that provides a realization of two competing length scales for anisotropic interactions. Oblate ellipsoids, which are often invoked in coarse-grained descriptions of discotic molecules, are therefore promising building blocks for self-assembling helical structures. Hard ellipsoids of revolution are not suitable as they do not form a columnar phase (21). It is therefore instructive to explore routes to helicity with soft ellipsoids of revolution. We consider two pair potentials of this sort: (*i*) a suggestion by Paramonov and Yaliraki (PY) (22); and (*ii*) a version of the Gay–Berne (GB) potential (23), modified by Bates and Luckhurst (BLmGBD) (24) for uniaxial oblate ellipsoids. We focus here on parameterizations where the face-to-face configuration of two uniaxial oblate ellipsoids is favored over the edge-across-edge configuration (Fig. S1 of the *SI Appendix*). This bias is

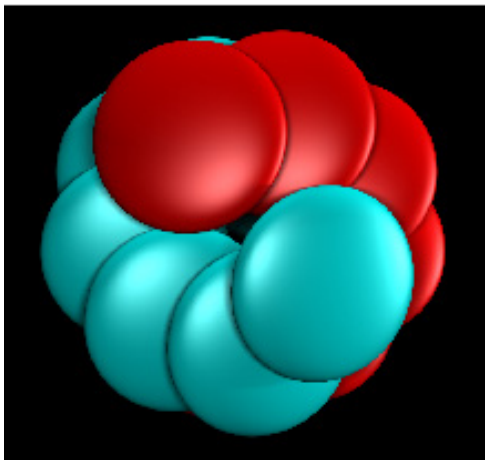

**Fig. 2.** Global minimum for a cluster of 13 axially symmetric discoids bound by the PY potential. A double-helical structure emerges for the following parameter set: $a_{11} = a_{12} = 0.5$, $a_{13} = 0.15$, $a_{21} = a_{22} = 0.45$, $a_{23} = 0.19$, $\sigma_0^{PY} = 1$, and $\varepsilon_0^{PY} = 1$.

conducive to columnar stacking, as for $\pi-\pi$ interactions in aromatic systems (7–9).

The PY potential is a generalization of the LJ potential for ellipsoidal particles, based on the distance of closest approach of two ellipsoids with given orientations, as measured by the elliptic contact function (22). For identical ellipsoids, the potential involves a set of eight parameters, six of them, $\{a_{1k}\}$ and $\{a_{2k}\}$ ($k = 1,2,3$), defining two different shape matrices for the repulsive and attractive parts of the interaction, and the other two, $\sigma_0^{PY}$ and $\varepsilon_0^{GB}$, defining the length and energy scales, respectively. For the PY model, we tune the parameters so that the lowest-energy configuration for two axially symmetric discoids involves an offset geometry (8) (Fig. S1 of the *SI Appendix*). Fig. 2 shows that for an appropriate parameter set the global minimum for a 13-discoid cluster has a double-helical morphology. In this case, the stacked helical structure appears without the long-range interactions (25).

We now illustrate the emergence of chiral structures for assemblies of axially symmetric discoids bound by the BLmGBD potential, even when the lowest-energy configuration for two discoids does not correspond to an offset geometry. The BLmGBD potential makes use of the orientation-dependent molecular shape parameter $\sigma$ and the energy parameter $\varepsilon$ to model the interaction between two uniaxial oblate ellipsoids (24), each having a single-site representation. The potential involves four essential parameters, i.e., $\{\kappa, \kappa', \mu, \nu\}$. Here $\kappa$ is the aspect ratio of the ellipsoid, $\kappa' = \varepsilon_{ee}/\varepsilon_{ff}$, where $\varepsilon_{ee}$ is the depth of the minimum of the potential for a pair of ellipsoids aligned parallel in the edge-across-edge configuration, and $\varepsilon_{ff}$ is the corresponding depth for the face-to-face alignment. The other two parameters control the orientation-dependent depth of the potential. Two additional parameters, $\sigma_0^{GBD}$ and $\varepsilon_0^{GBD}$, define the length and energy scales, respectively. Here we set $\kappa = 0.345$ from the parameterization of the GB potential that mimics the interaction between two molecules of triphenylene (26), which is known to form the core of many discotic mesogens (2). Fig. 3 shows putative global minima for 13-discoid clusters bound by the BLmGBD potential for different sets of parameters. We fixed $\kappa = 0.345$, $\kappa' = 0.2$, and $\nu = 1$, and varied $\mu$. For $\mu = 0$, even though two length scales are involved for the closest approach, there is no bias between the face-to-face and edge-across-edge configurations for a pair of discoids. The global minimum is then a squashed icosahedron for $n = 13$ and a squashed double icosahedron for $n = 19$. For $\mu \neq 0$, the bias toward the face-to-face configuration, set by $\kappa' = 0.2$, ensures columnar stacking. As $\mu$ increases, this bias does not change, but the orthogonal approach gradually becomes favored over the edge-on arrangement (see Fig. S1 of the *SI Appendix* for $\mu = 2$). For $\mu \geq 0.4$, chiral character for the columnar arrangements starts to emerge.

For $n = 38$, we find a central column around which there are six other stacks that form a regular helical arrangement (Fig. 4*A*). Handedness is clearly established upon symmetry breaking, which in turn is caused by the packing of soft discoids driven by the two competing length scales. Right- and left-handed structures exist with equal energies, and similar chiral structures have been found for $n = 49$ (Fig. 4*B*). When the parameter space is explored for $n = 49$, the chirality of the self-assembled structures is evident over a wide regime (see *SI Text* and Figs. S4–S6 of the *SI Appendix*). In particular, the relative twist of the adjacent stacks is found to vary nonmonotonically as the aspect ratio $\kappa$ changes. This observation lends firm support to the idea that competing interactions involving two length scales form a route to the emergence of chiral structures. Although our results here are for relatively small clusters, where surface effects are important, the insight they provide is also relevant for bulk systems (27).

In conclusion, drawing inspiration from nature, we have demonstrated how chiral structures can emerge for building blocks bound by the interplay between two competing length scales. Factors suggested previously to induce chiral structures, such as competing dipolar and quadrupolar interactions (28), or particle shape anisotropy (25), are consistent with this view, which the present study establishes via explicit case studies. The competing interactions might be tuned in practice through aromatic $\pi-\pi$ stacking (7), hydrogen bonding (29), metal ligation (30), or by the application of a field (17). The simplest example we have found involves an axially symmetric discoid as the building block. This observation further demonstrates that noncentrosymmetric particles and chiral fields are not necessary for helices to be favorable (31, 32). We believe that the insights

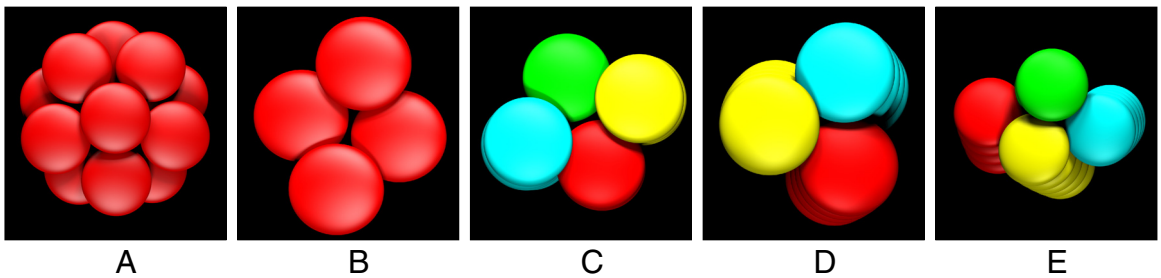


**Fig. 3.** Global minima for clusters of axially symmetric discoids bound by the BLmGBD potential. (*A–D*) Here, for 13 discoids $\kappa = 0.345$, $\kappa' = 0.2$, and $\nu = 1$, and $\mu$ varies as follows: $\mu = 0$ (*A*); $\mu = 0.2$ (*B*); $\mu = 0.4$ (*C*); and $\mu = 2$ (*D*). (*E*) The same parameter set as in *D*, but for 20 discoids. The stacks are colored differently for the chiral structures.

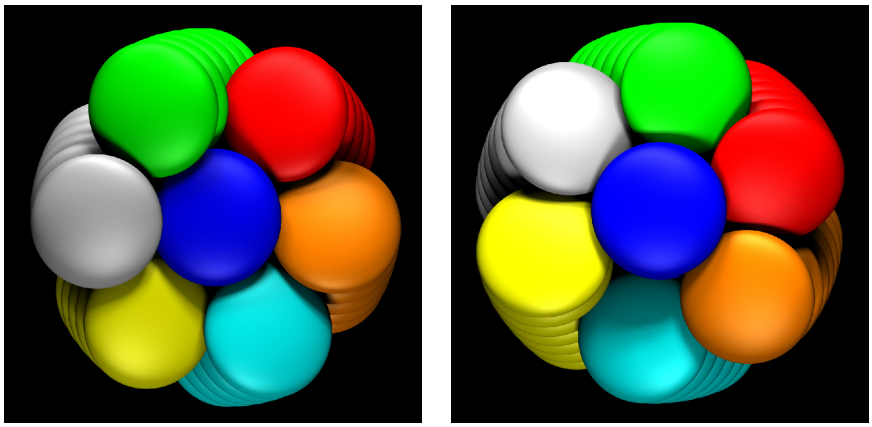


**Fig. 4.** Global minima for clusters of axially symmetric discoids bound by the BLmGBD potential. Here, $\kappa = 0.345$, $\kappa' = 0.2$, $\mu = 2$, and $\nu = 1$ for two different cluster sizes: $n = 38$ (*A*) and $n = 49$ (*B*). Different colors are used to distinguish between the stacks.

our results provide are sufficiently general to aid rational design of materials with helical order, especially for optoelectronic applications (2–4).

## Materials and Methods

We used the basin-hopping (15) approach to identify the global minima. This method is based on hypersurface deformation where the transformation of the potential energy surface neither changes the global minimum nor the relative energies of any local minima. We accept a structure as the global minimum for a cluster if at least five different runs starting from random configurations at a given size produce the same lowest minimum.

**ACKNOWLEDGMENTS.** We thank Prof. A. J. Stone and Dr. M. A. Miller for helpful discussions. D.C. and S.N.F. gratefully acknowledge support from the Oppenheimer Fund and Gates Cambridge Trust, respectively.

1. Watson JD, Crick FHC (1953) A structure for deoxyribose nuclei acid. *Nature* 171:737–738.
2. Adam D, et al. (1994) Fast photoconduction in the highly ordered columnar phase of a discotic liquid crystal. *Nature* 371:141–143.
3. Schmidt–Mende L, et al. (2001) Self-organized discotic liquid crystals for high-efficiency organic photovoltaics. *Science* 293:1119–1122.
4. Percec V, et al. (2002) Self-organisation of supramolecular helical dendrimers into complex electronic materials. *Nature* 419:384–387.
5. Goodby JW (1991) Chirality in liquid crystals. *J Mater Chem* 1:307–318.
6. Fontes E, Heiney PA, de Jeu WH (1988) Liquid-crystalline and helical order in a discotic mesophase. *Phys Rev Lett* 61:1202–1205.
7. Engelkamp H, Middelbeek S, Nolte RJM (1999) Self-assembly of disc-shaped molecules to coiled-coil aggregates with tunable helicity. *Science* 284:785–788.
8. Azumaya I, et al. (2004) Absolute helical arrangement of stacked benzene rings: Heterogeneous double-helical interaction comprising a hydrogen-bonding belt and an offset parallel aromatic-aromatic interaction array. *Angew Chem Int Ed* 43:1360–1363.
9. Wang Z, Enkelmann V, Negri F, Müllen K (2004) Rational design of helical columnar packing in single crystals. *Angew Chem Int Ed* 43:1972–1975.
10. Zhang S (2003) Fabrication of novel biomaterials through molecular self-assembly. *Nat Biotechnol* 21:1171–1178.
11. Service RF (2005) How far can we push chemical self-assembly. *Science* 309:95.
12. Whitesides GM, Boncheva M (2002) Beyond molecules: Self-assembly of mesoscopic and macroscopic components. *Proc Natl Acad Sci USA* 99:4769–4774.
13. Glotzer SC, Solomon MJ (2007) Anisotropy of building blocks and their assembly into complex structures. *Nat Mater* 6:557–562.
14. Wales DJ, Scheraga HA (1999) Global optimization of clusters, crystals, and biomolecules. *Science* 285:1368–1372.
15. Wales DJ, Doye JPK (1997) Global optimization by basin-hopping and the lowest energy structures of Lennard–Jones clusters containing up to 110 atoms. *J Phys Chem A* 101:5111–5116.
16. Woodley SM, Catlow R (2008) Crystal structure prediction from first principles. *Nat Mater* 7:937–946.
17. Zerrouki D, Boudri J, Pine D, Chaikin P, Bibette J (2008) Chiral colloidal clusters. *Nature* 455:380–382.
18. Chakrabarti D, Wales DJ (2009) Simulations of rigid-bodies in an angle-axis framework. *Phys Chem Chem Phys* 11:1970–1976.
19. Miller MA, Wales DJ (2005) Novel structural motifs in clusters of dipolar spheres: Knots, links, and coils. *J Phys Chem B* 109:23109–23112.
20. Dudowicz J, Freed KF, Douglas JF (2004) Flory–Huggins model of equilibrium polymerization and phase separation in the Stockmayer fluid. *Phys Rev Lett* 92:045502.
21. Frenkel D, Mulder BM (1985) The hard ellipsoid-of-revolution fluid. *Mol Phys* 55:1171–1192.
22. Paramonov L, Yaliraki SN (2005) The directional contact distance of two ellipsoids: Coarse-grained potentials for anisotropic interactions. *J Chem Phys* 123:194111.
23. Gay JG, Berne BJ (1981) Modification of the overlap potential to mimic a linear site-site potential. *J Chem Phys* 74:3316–3319.
24. Bates MA, Luckhurst GR (1996) Computer simulation studies of anisotropic systems. XXVI. Monte Carlo investigations of a Gay–Berne discotic at constant pressure. *J Chem Phys* 104:6696–6709.
25. Fejer SN, Wales DJ (2007) Helix self-assembly from anisotropic molecules. *Phys Rev Lett* 99:086106.
26. Emerson APJ, Luckhurst GR, Whatling SG (1994) Computer simulation studies of anisotropic systems XXIII. The Gay–Berne discogen. *Mol Phys* 82:113–124.
27. Chakrabarti D, Wales DJ (2008) Tilted and helical columnar phases for an axially symmetric discoidal system. *Phys Rev Lett* 100:127801.
28. Van Workum K, Douglas JF (2006) Symmetry, equivalence, and molecular self-assembly. *Phys Rev E* 73:031502.
29. Verl V, Huc I, Khoury RG, Krische MJ, Lehn J-M (2000) Interconversion of single and double helices formed from synthetic molecular strands. *Nature* 407:720–723.
30. Evans OR, Lin W (2002) Crystal engineering of NLO materials based on metal–organic coordination networks. *Acc Chem Res* 35:511–522.
31. Maritan A, Micheletti C, Trovato A, Banavar JR (2000) Optimal shape of compact strings. *Nature* 406:287–290.
32. Pokroy B, Kang SH, Mahadevan L, Aizenberg J (2009) Self-organization of a mesoscale bristle into ordered, hierarchical helical assemblies. *Science* 323:237–240.